euronoise

Noise computation of an axisymmetric free jet using general purpose CFD code

Péter Tóth and Máté Márton Lohász

Dep. of Fluid Mechanics, Budapest Univ. of Technology and Economics, Bertalan Lajos street 4-6, 1111 Budapest, Hungary
toth@ara.bme.hu

The increasing interest in the noise prediction of the turbulent flows is leading the general purpose Computational Fluid Dynamics (CFD) software developers to integrate noise predicting methods into their code. However the aeroacoustic simulation of free shear flows, where the mean source of noise is the turbulent fluctuations in the free space is challenging with a general purpose CFD application. The aim of this work is to investigate the capabilities of commercial CFD software in the field of noise prediction of free shear flows. The important acoustical properties of a low Reynolds number, low Mach number axisymmetric (2D) jet is computed by means of hybrid Computational Aeroacoustic method using Fluent. The noise source is computed instantaneously using the compressible solver of the code, and the far field acoustical data is evaluated by the Ffowcs-Williams-Hawkings acoustical analogy. The results is compared to the Direct Numerical Simulation data can be found in the literature.

1 Introduction

The direct computation of the aerodynamically generated sound can be useful, when the acoustic source mechanism of the fluid motion is under investigation. Using this method on a relatively simple flow configurations basic information can be gathered on the noise source properties of vortex rollup, vortex pairing [8] and vortex shedding [3] etc. events. These direct flow computations are often calculated by specialised in house codes. With these computation tools accurate simulations can be made but the handling of complex flow configuration is usually problematic. On the other hand the general purpose Computational Fluid Dynamics (CFD) applications – used mostly in industrial applications – are designed to capture the most energetic motion of the fluid flows. Therefore these applications are using robust but less accurate numerical methods. The direct simulation of the acoustic waves, that has a relatively small amplitude beside the turbulent motion, with these less accurate numerical capabilities is not evident. The aim of this paper is to investigate the capabilities of a commercial CFD code Fluent in the field of direct computation the sound field radiated by an axisymmetric shear layer.

2 Numerical setup

Numerical simulation of an axisymmetric free jet flow was carried out at discharge Reynolds number of $Re = U_0 R_0/\nu = 2500$ and Mach number $Ma = U_0/a_\infty = 0.4$, where U_0 is the inlet maximum velocity, R_0 is the nozzle radius and a_∞ is the ambient sound speed. These parameters resemble to the Direct Numerical Simulation of [5] and [4]. The compressible Navier-Stokes equations were solved in the near field of the jet with the commercially available solver Ansys Fluent 12.0.3 (beta). The ideal gas law was used as the constitutive equation. The ratio of specific heats was $\gamma = 1.399$, the thermal conductivity was $\lambda = 0.0242 W/mK$, and the specific gas constant was $R = 287.0379 J/kgK$. The acoustical far field data was evaluated by the Ffowcs-Williams and Hawkings (hereafter FWH) analogy, which is also available in the solver. The extension to the far field was completed with permeable control surfaces placed into the simulation domain.

2.1 Domain and grid parameters

The sketch of the simulation domain is depicted in Fig1. The simulation domain is rectangular and extends up to $x_{max} = 50R_0$ in the streamwise (x) direction and up to $r_{max} = 30R_0$ in the radial (r) direction. In this domain a $10R_0$ width zone is separated along the outflow boundaries (located at $x = x_{max}$ and $r = r_{max}$) for the implementation of the sponge type non reflective boundary condition [1]. In this region the simulation results are not considered. The inlet boundary condition is prescribed at $x = 0$. Three control surfaces (Surface 1, 2, 3 as shown in Fig1) are placed in the physical domain for the purpose of exporting sound source data into the FWH solver. The surfaces are located at $r = 5R_0$, $r = 10R_0$ and $r = 16R_0$ respectively. The simulation domain is discretised with block structured mesh constructed from non uniformly distributed quadrilateral cells. The physical domain is discretised with 224 cells in the streamwise and 96 cells in the radial directions. The smallest cell in the domain is located at the inflow boundary ($x = 0$, $r = R_0$) with the extend of $\delta_x = 0.05R_0$, $\delta_r = 0.04R_0$ in the streamwise and radial direction respectively. The grid is stretched from this point along the streamwise and radial directions. In the physical domain the maximum cell size change is 1.25 and the equiangle skewness [2] is 0.14. The ratio of the maximum and minimum cell size in the streamwise and radial directions are 5.4 and 5 respectively. The overall cell number is 32004.

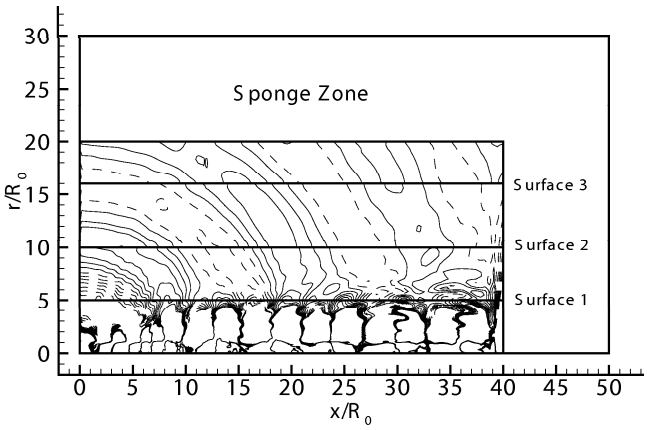

Figure 1: Simulation domain with the three FWH control surfaces and dilatation countours depicted in the physical domain. (15 equally spaced isolines between $\pm 2.96 \times 10^{-4} U_0/R$. Dashed lines denotes negative values.)

2.2 Boundary and initial conditions

At the inflow boundary the axial velocity distribution and the temperature profile is defined. In order to control the roll up of the shear layer the prescribed hyperbolic tangent velocity profile [4] is harmonically excited:

$$u = \left(\frac{U_0}{2} + u'\right)\left\{1 - th\left[\frac{R_0}{4\theta_0}\left(\frac{r}{R_0} - \frac{R_0}{r}\right)\right]\right\} \quad (1)$$

$$u' = \frac{U_0}{2} a \sum_{n=0}^{2} sin(\frac{2\pi f_0}{2^n} t) \quad (2)$$

, where $\theta_0 = 0.1R_0$ is the initial momentum thickness, ω_0 is the fundamental frequency calculated with Strouhal number $St = f_0 R_0/U_0 = 0.218$, which is the same as in [5], [4] and $a = 0.01$. The temperature profile is prescribed using the Crocco-Busemann relation [7]:

$$T = T_0\left[1 + \frac{\gamma - 1}{2} Ma^2 \frac{u}{U_0}\left(1 - \frac{u}{U_0}\right)\right] \quad (3)$$

, where T_0 is the temperature of the ambient fluid. Using these inflow values a mass flow boundary condition of [2] is applied using the locale pressure in the constitutive equation for the density. At $r = 0$ axis boundary condition is defined. The outflow boundary condition is treated as a constant pressure boundary using the value in the ambient fluid. Since this boundary condition in itself can not model the far field behaviour of the compressible fluid, additional technique is needed to avoid the acoustic wave reflections. The sponge type boundary condition [1] is implemented in the zone depicted in Fig1 to this end. Source terms (S) are defined for the flow equations in the following form:

$$S(x, r) = -\alpha(x, r)\left[q(x, r) - q_{ref}(x, r)\right] \quad (4)$$

, where q is the primary variable of the equation (i.e. density, momentum components and the total energy), q_{ref} is the reference value, and α is the sponge strength factor. The reference values are obtained by running the simulation without source terms and evaluating mean flow statistics with an averaging time of $1538R_0/U_0$. The sponge strength factor is defined as follows:

$$\alpha_x = \frac{1}{2}\alpha_{max}\left[1 - th\left(\frac{x_{max} - h - x}{ch}\right)\right] \quad (5)$$

$$\alpha_r = \frac{1}{2}\alpha_{max}\left[1 - th\left(\frac{r_{max} - h - r}{ch}\right)\right] \quad (6)$$

$$\alpha(x, r) = max\left(\alpha_x, \alpha_r\right) \quad (7)$$

, where h is the width of the profile, $c = 0.28957$ is a predefined constant determined to ensure the smoothness of profile perpendicular to the outflow boundaries, and α_{max} is the maximal value of the sponge strength factor. The value of $h = 8R_0$ was chosen in this simulation, which means that at the inner boundary of the $10R$ width sponge zone the sponge strength factor value is approximately 15% of α_{max}. The sufficent value of α_{max} to avoid significant wave reflexions is in the order of 10^5 determined by previous parameter studies. In this paper results using $\alpha_{max} = 2 \times 10^5$ will be presented.

The complete simulation process is composed from 4 stages. The simulation is initialised to quiescent fluid state. After an approximately $815R_0/U_0$ long spin up computation, without the sponge zone activated, the mean flow statistics is collected during the $1538R_0/U_0$ long time period. Then the sponge zone is activated and the flow is relaxed to the statistically stationary state with a $316R_0/U_0$ long computation. The acoustical and flow data were considered from this point.

2.3 Solver setup

During the simulation the density based solver of Fluent was used. Explicit spatial and temporal discretisation was used with second order upwind and four stage Runge-Kutta scheme respectively [2]. The flux handling was Roe-FDS and the gradients were evaluated by cell based Green-Gauss formulation [2]. CFL number of 1 was used. These solver settings performed with acceptable error and reasonable computational requirements in a $2D$ acoustic pulse propagation test case [6].

The applied Ffowcs-Williams and Hawkings solver was the one implemented in Fluent. This solver is using $3D$ Green function to evaluate the far field data. This solver can be used also for $2D$ slab symmetric flow simulations since the third dimensional (linear) extend of the source can be defined trough the source correlation length parameter. This formulation was used in our axisymmetric simulation case by setting the correlation length to $0.2R_0$. The source data was exported along the predefined surfaces and acoustic data calculated as post processing task.

3 Results

The simulation results were examined in terms of near-field instantaneous motion, far-field acoustic spectra and directivity properties of the jet.

3.1 Flow field

Vorticity contours of the flow field can be seen in Fig2 with time intervals $\Delta t = 1/(4f_0)$. The flow field is time periodic. A pairing process take place in the computation domain between about $10R_0 < x < 16R_0$ corresponding to the first subharmonic frequency. The merged vortices are convected downstream while their amplitude is slightly decreasing. The results are in agreement with the simulation of [5]. However the pairing procedure is $2R_0$ upstream in the present simulation, and the vortices after the pairing have lower vorticity level. The difference in the streamwise position can be partially attributed to the minor differences in the inlet boundary condition. The lower streamwise mesh resolution can be responsible for the faster decay of the vorticity (since the increased dissipation of the numerical scheme) and also for the difference in position of the pairing.

In Fig3 the pressure fluctuation is depicted at $r = R_0$ radial position in the centre of the shear layer. The signal is presented separately for the dominant sub- and sup- harmonic frequencies. This result can be compared with the Fig5a of [5], where the spectral components of the velocity fluctuations are presented. The fundamental frequency component is dominating in the region of $x < 8R_0$ corresponding to vortex roll up. Downstream of this location the first subharmonic ($f_0/2$) generated by the paring process is exceeding all other frequencies.

The peak value corresponding to this frequency is located around $x = 13R_0$, where the fundamental frequency has a local maximum as well. The decay downstream the peak is apparently stronger than the one found by [5], this observation agree with the one find for the vorticity. The sponge zone effectively damps out all the frequencies up to the outflow.

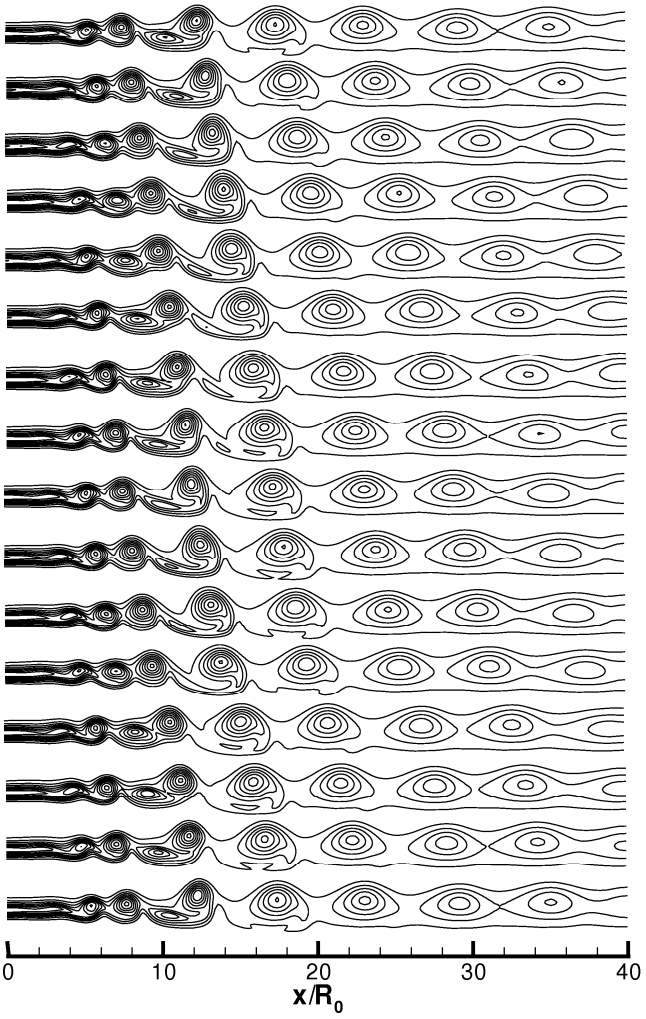

Figure 2: Time elvolution of vorticity contours with equally spaced time intervals of $\Delta t = 1/(4f_0)$. Ten contour levels range from 0 to $2.8U_0/R_0$.

3.2 Dilatation

The dilatation contours can be seen in Fig1. In the flow field the dilatation contours show the quadrupole structures located around the vortices. The acoustic near-field dilatation shows approximately spherical wave fronts. The main sound generation region seems to be placed at the origin of the coordinate system, this is also pronounced in the fact that the wave fronts are perpendicular to the inlet boundary. Both the simulation of [4] and [5] predict the sound source more downstream and waves are propagating upstream at $x = 0$ position.

3.3 Acoustic spectra

In Fig4 the spectra of the pressure is evaluated at $x = 16R_0$, $r = 16R_0$.

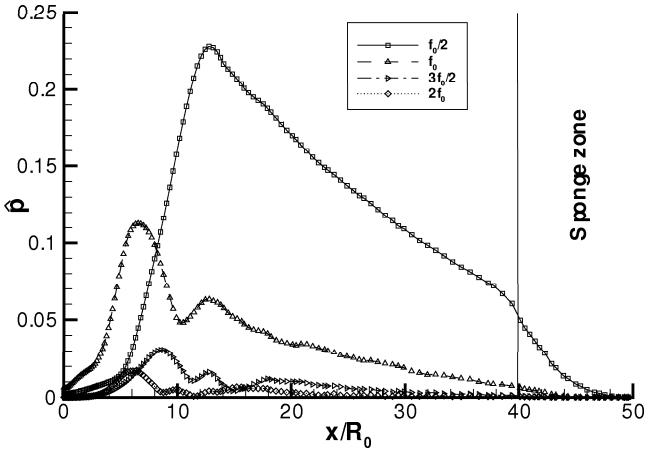

Figure 3: Fourier transform amplitudes of pressure, along the line $r = R_0$.

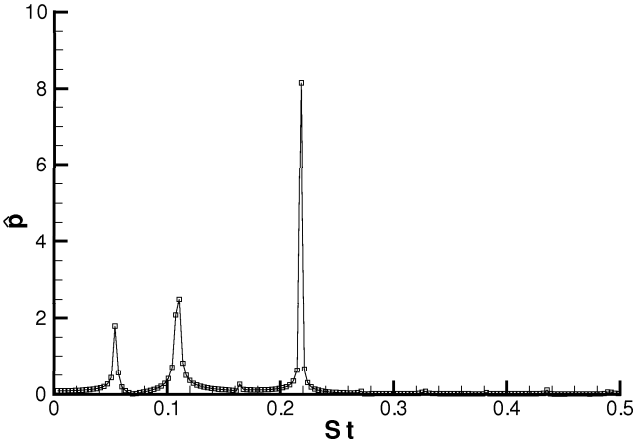

Figure 4: Acoustic pressure amplitude spectra at $x = 16R_0$, $r = 16R_0$. Computed directly from the simulation data.

In this spectra the forced harmonics are present, with different amplitudes. This is a difference comparing to the simulation of [5], where higher harmonics of the fundamental frequencies are also present up to $2f_0$. Apparently the sup harmonics are damped more strongly in the present simulation, since in the source field they were predicted as it was presented in Fig3.

Considering the simulation spectra of [4] (Fig7b) which is at different distance but at similar direction, the amplitude distribution of the frequencies are different from the present results, since their results showed approximately the same amplitude level in all three dominant frequencies.

The far field acoustic pressure was computed using the FWH analogy at position $x = 60R_0$, $r = 60R_0$, and the Fourier transform of the signal can be seen in Fig5.

Beside of the three forced harmonics only the $3/4f_0$ frequency is dominantly present additionally in the result with a small amplitude.

Significant amplitude discrepancy can be also observed if the FWH computation is accomplished by using the three different source surfaces. The amplitudes are higher, if the surfaces placed at larger radial coordinates were used as source. This suggests that there are sound sources located outside of the 1^{st} and 2^{nd} surfaces, and their contribution is only accounted for if the

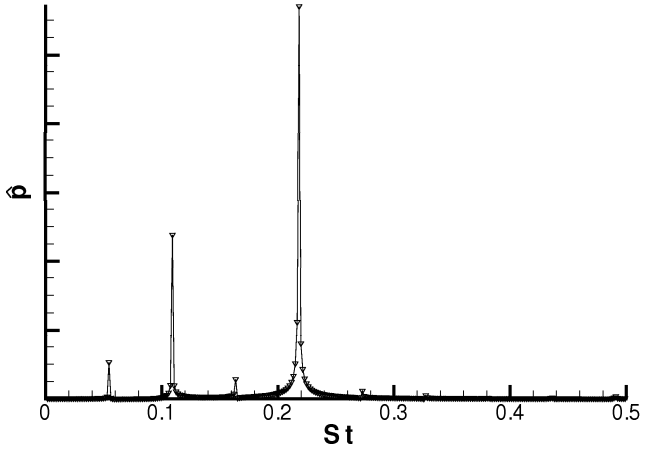

Figure 5: Acoustic pressure amplitude spectra at $x = 60R_0$, $r = 60R_0$. Calculated with the second FWH control surface.

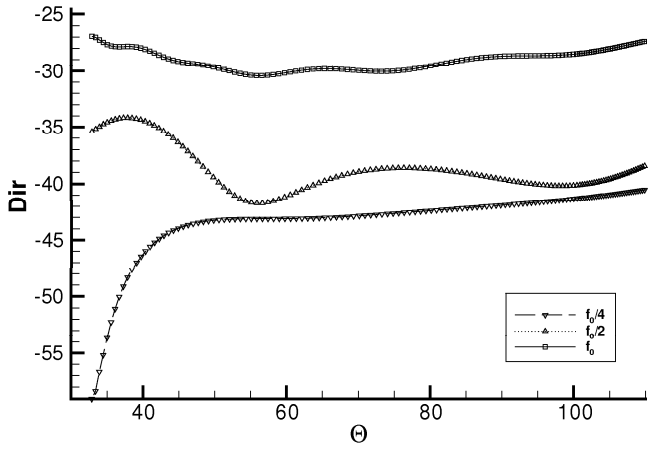

Figure 6: Directivity magnitudes as the function of angle from the axis

the source surface is located at higher radial distance. It should be mentioned that higher frequency spikes can also be observed in the Fourier transform around $St = 2$ in the case of the far field acoustic computation is based on the first control surface data.

3.4 Sound field directional characteristic

The directional character of the sound field is examined using the quantity defined as:

$$Dir(\Theta) = 10log_{10}\frac{\hat{p}^2 R_c^2}{sin^2\Theta} \tag{8}$$

, where $\hat{p}$ is the Fourier transform amplitudes, R_c is the radial coordinate of the sampling line, and Θ is the angle of the sampling point measured from the axis. The apparent source location was chosen as $x = 0$, $r = 0$. The directivity diagram exported for the three dominant frequencies can be seen in Fig6. The fundamental frequency is dominating the whole acoustic field with approximately constant value for all directions. The $f_0/2$ component shows local minimum at $\Theta = 40°$, which is expected since this frequency is dominantly radiated by the vortex pairing process which has a quadrupole direction character [8]. However the smaller amplitude level of this quadrupole source is overwhelmed by the strong spherically symmetric radiation of the f_0 component in the overall sound pressure directivity field. This can be also verified by the dilatation field in Fig1, which is dominated by the fundamental frequency component. The $f_0/4$ subharmonic component shows the lowest radiation level and it is rapidly vanishing at low angles (below $\Theta = 45°$).

4 Conclusion

In this paper an axisymmetric low Reynolds number subsonic jet flow and its radiated sound field have been investigated using a commercial Computational Fluid Dynamics software Fluent 12.0.3. The flow field shows agreement with the literature data. Beside of this agreement in the flow features the vorticity of the merged rollers is decaying more rapidly than it was in the Direct Numerical Simulation of [5] and [4]. This behaviour pointed out that mesh dependency of the presented calculations needs to be investigated further.

In terms of the radiated acoustic field the present simulation shows the dominance of the fundamental frequency. However this was not the case in the simulation of [5] and [4]. This frequency showed an approximately spherically symmetric radiation character originated from the symmetry axis at the inflow boundary. Beside of this, the dominant vortex pairing sound showed the expected quadrupole directivity but with lower amplitude than the fundamental frequency.

The Ffowcs-Williams and Hawkings method was also used to predict the far field sound. The frequencies were well predicted but deficiencies were found from the perspective of the amplitudes. For this reason the applicability of the Fluent's built in Ffowcs-Williams and Hawkings far field sound extension method (which is originally implemented for slab symmetrical $2D$ flows) in a axisymmetric simulation case needs to be further investigated.

References

[1] D. J. Bodony. Analysis of sponge zones for computational fluid mechanics. *Journal of Computational Physics*, 212:681–702, 2006.

[2] Fluent, Inc. *Fluent 6.3 User's Guide*, January 2006.

[3] O. Inoue and N. Hatekeyama. Sound generation by a two-dimensional circular cylinder in a uniform flow. *Journal of Fluid Mechanics*, 471:285–314, 2002.

[4] X. Jiang, E. J. Avital, and K. H. Luo. Direct computation and aeroacoustic modelling of a subsonic axisymmetric jet. *Journal of Sound and Vibration*, 270:525–538, 2004.

[5] B. E. Mitchell, S. K. Lele, and P. Moin. Direct computation of the sound generated by vortex pairing in an axisymmetric jet. *Journal of Fluid Mech*, 383:113–142, 1999.

[6] P. Tóth, A. Fritzsch, and M. M. Lohász. Application of computational fluid dynamics softwares for 2d acoustical wave propagation. In *Gépészet2008*, 29-30 May 2008.

[7] A. Uzun, A. S. Lyrintzis, and G. A. Blaisdell. Coupling of integral acoustics methods with les for jet noise prediction. *International Journal ofAeroacoustics*, 3(4):297–346, 2005.

[8] R. Verzicco, A. Iafrati, G. Riccardi, and M. Fatica. Analysis of the sound generated by the pairing of two axisymmetric co-rotating vortex rings. *Journal of Sound and Vibration*, 200(3):347–358, 1997.